KIGAS Vol. 12, No. 3, September, 2008
(Journal of the Korean Institute of Gas)

Measurements on Effects of Locations of Obstacles in an Explosion Chamber

†Jae Beom Han · Young Soon Lee* · Dal Jae Park**

*Department of Safety Engineering, Seoul National University of Technology, Seoul 139-743, Korea
**Research Center for System Safety, Seoul National University of Technology, Seoul 139-743, Korea
(Received 23. July. 2008, Revised 5. September. 2008, Accepted 5. September. 2008)

요 약

폭발챔버에서 전파하는 화염과 장애물 위치 및 형태에 따른 상관관계를 조사하기 위해 폭발실험을 수행하였다. 챔버내에 장애물 설치 위치는 점화원으로부터 상부로 200 mm, 500 mm, 800 mm 높이로 변화를 주어 설치하였고, 장애물 형태는 삼각기둥, 사각기둥 및 원통형으로 변화시켰다. 전파하는 화염과 장애물 위치 및 형태에 따른 상관관계를 조사하기 위해 고속카메라를 사용하였다. 고속카메라로 얻어진 화염 이미지로부터 장애물 주위의 국부 화염속도 및 그 화염속도의 확률밀도함수가 계산되었다. 실험결과, 장애물이 800 mm에 위치하였을 때 화염속도 및 폭발압력이 가장 높게, 200 mm에서는 가장 낮게 나타났다. 이러한 결과는 폭발거동 특성이 장애물 위치에 큰 의존성을 가지는 것으로 해석될 수 있다. 또한, 장애물 형태가 삼각형이었을 때 화염속도 및 폭발압력이 가장 높게, 원형에서는 가장 낮게 나타났다.

Abstract – Measurements were performed to investigate the effects on flame and pressure development by varying locations of multiple obstacles in a top-venting explosion chamber. The chamber dimension was 1000 mm in height with a 700 × 700 mm^2 cross-section and a rectangular vent area of 700 × 210 mm^2. Three different multiple obstacles with blockage ratio of 30% were used by changing from 200 mm, 500 mm to 800 mm in heights within the chamber. Temporally resolved flame front images were recorded by a high speed camera to investigate the interaction between the propagating flame and the obstacles. The results showed that the triangular bar caused the fastest flame developments at given times whereas the lowest was obtained with the cylindrical bar. It was also found that local flame displacement speeds of different obstacles were sensitive to the locations of obstacles. The local speed becomes larger in going from 200 mm, to 500 mm and to 800 mm in heights. The obstacles in height of 800 mm yielded the highest overpressure whereas the lowest was in height of 200 mm.

Key words : obstacle locations, flame propagation, pressure

I. Introduction

Gas explosions occurring in congested and partially opened regions have been treated as of special concern due to potential loss of life, asset, business interruption risks, etc. The severity of such explosions is mainly dependent on flame acceleration levels. Over the last decade, considerable effort has been concentrated on the development of experimental [1-5] and computational fluid dynamics (CFD) tools [6,7] for studying the flame acceleration. It is well understood that local flame acceleration results from a complex interaction between a freely propagating flame front and a local blockage caused by the presence of obstacles. In recent years the effects of obstacle types on flame propagation and explosion pressure were examined by many investigators [8-11]. Their results showed that both the flame and pressure were sensitive to both the obstacle types and the blockage ratios. This is due to different turbulence levels generated by vortex shedding and local wake/recirculation behind obstacle.

However, although the results of the experiments and the modeling revealed that the interaction between propagating flames and obstacles is a key phenomenon in determining the severity of gas explosions, more detailed data of the influences of obstacle type in different locations on both the flame and pressure development have not been clearly examined.

The present work aims at investigating the underlying mechanisms of local flame/obstacle interactions

Corresponding author:pdj70@snut.ac.kr(박달재)

by varying the positions of obstacles within a laboratory explosion chamber. This work includes data of global and local flame developments, local flame displacement speed and pressure development.

II. Experimental and Data Processing

The fuel-air mixture, apparatus and experimental methods used in this work are the same with the measurements described in previous work [12]. Fig. 1 shows a schematic of the experimental set-up. The dimensions of explosion chamber are 1000 mm in height, with a $700 \times 700\ mm^2$ cross-section and a rectangular top-venting area of $700 \times 210\ mm^2$. The chamber is made of 20 mm thick transparent perspex. Three different multiple obstacles: cylindrical, square and triangular bars with blockage ratio of 30% were employed inside the chamber. The locations of obstacles were varied from 200 mm, 500 mm up to 800 mm in heights within the chamber. The pitch (the relative distance between two successive obstacles) of multiple obstacles was 175 mm. Full details of all the obstacles used are given in Table 1. In the experiments, the methane concentration in air was kept at $10 \pm 0.2\%$. The pressure inside the chamber was monitored by one pressure transducer mounted on the top wall of the chamber 20 mm from the chamber exit. Each test was repeated at least five times in order to ensure reproducibility. The results were averaged and the average values were presented. The reproducibility between all tests was found to be good: the error was 5% in time and 5% in pressure.

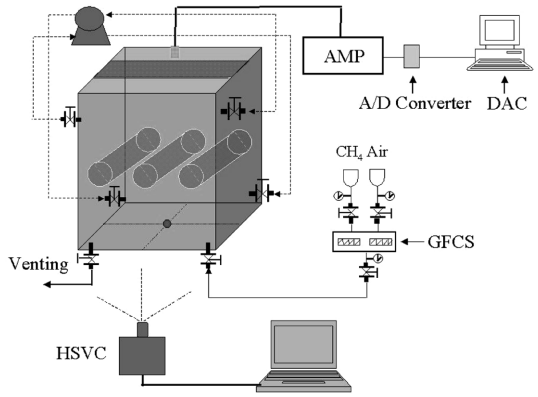

Fig. 1. Schematic of experimental arrangements.

Table 1. Configurations of all obstacles used.

Obstacles	Symbols	Dimensions (mm)	H (mm)
Multiple square bars	OP1MS	L700 × S70, P = 175	200
	OP2MS	L700 × S70, P = 175	500
	OP3MS	L700 × S70, P = 175	800
Multiple triangular bars	OP1MT	L700 × E.S.70, P = 175	200
	OP2MT	L700 × E.S.70, P = 175	500
	OP3MT	L700 × E.S.70, P = 175	800
Multiple circular bars	OP1MC	L700 × D70, P = 175	200
	OP2MC	L700 × D70, P = 175	500
	OP3MC	L700 × D70, P = 175	800

H: Distance from the bottom of chamber to the middle point of the obstacle1

The data processing techniques to investigate the local flame-front characteristics between the flame and the multiple obstacles were the same with those described in the previous paper [12]. A statistical approach was used for each identified stage in which the probability density functions of local flame displacement speed were determined from all data points along the flame front within the time frame of the stage. Three stages can be identified as the flame front interacts and propagates around the obstacle:

• Stage I - flow around the bottom face of the obstacle to the point where a shear wake forms (in the case of the triangular and square obstacles it is the corner of the bottom face, while it is the full diameter for the cylinder);

• Stage II - flame progression along the lateral sides of the square. This is not present for the other obstacles

• Stage III - the recirculation region behind the obstacle (from the corner of the top face for the square bar or the bottom face for the triangular bar, or the full diameter for the cylinder) until flame reconnection behind the obstacle.

There are two sources of errors in measuring local flame displacement speeds. The first source of error is the frame rate accuracy of the high-speed camera. The high-speed video camera operated at 500 frames per second has a resolution of 512×240 pixels. The camera sends a TTL timing pulse, which was captured by a digital oscilloscope with nanosecond accuracy. The signal was found to have a $\pm 0.01\%$ a timing error in measurement. The second is associated with the calculation of the normal line. For example, if the flame displacement is $S_{fd} = 5$ m/s and $\Delta t = 2$ ms, the distance Δt is equal to 10 mm (or 7.7 pixels) whereas the

precision is only one pixel, involving an error of 13%.

III. Results and Discussion

3.1. Flame Development

Fig. 2 shows an example of a sequence of high-speed images of global flame structures taken with multiple triangular obstacles at different heights in the chamber. The time shown presents the elapsed time after ignition and subsequent flame images are at 40 ms intervals.

Fig. 3 represents the temporal evolution of locally propagating flame front contours around different cross-section obstacles: square, triangle and circle in three different heights of 200 mm, 500 mm and 800 mm respectively within the chamber. In Figs. 3(a)-(c) subsequent flame fronts for the different obstacles are traced between 54 and 82 ms: the first contour is at t = 54 ms, and the last one at 82 ms, with a separation of 2 ms. In the case of Figs. 3(d)-(f) the flame contours are displayed from 120 to 138 ms and from 156 ms

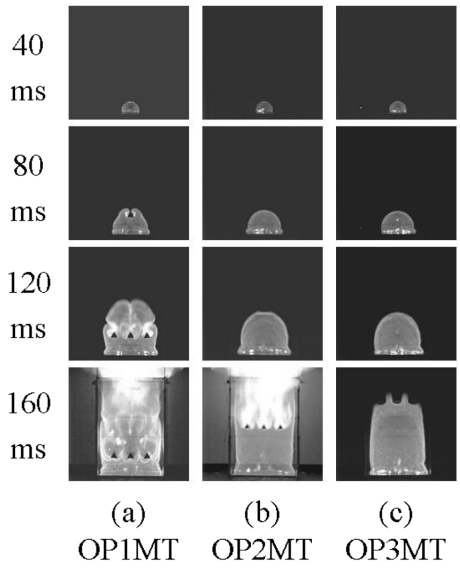

Fig. 2. Global flame propagation around multiple triangular obstacles in different positions within the chamber: (a) OP1MT, (b) OP2MT and (c) OP3MT.

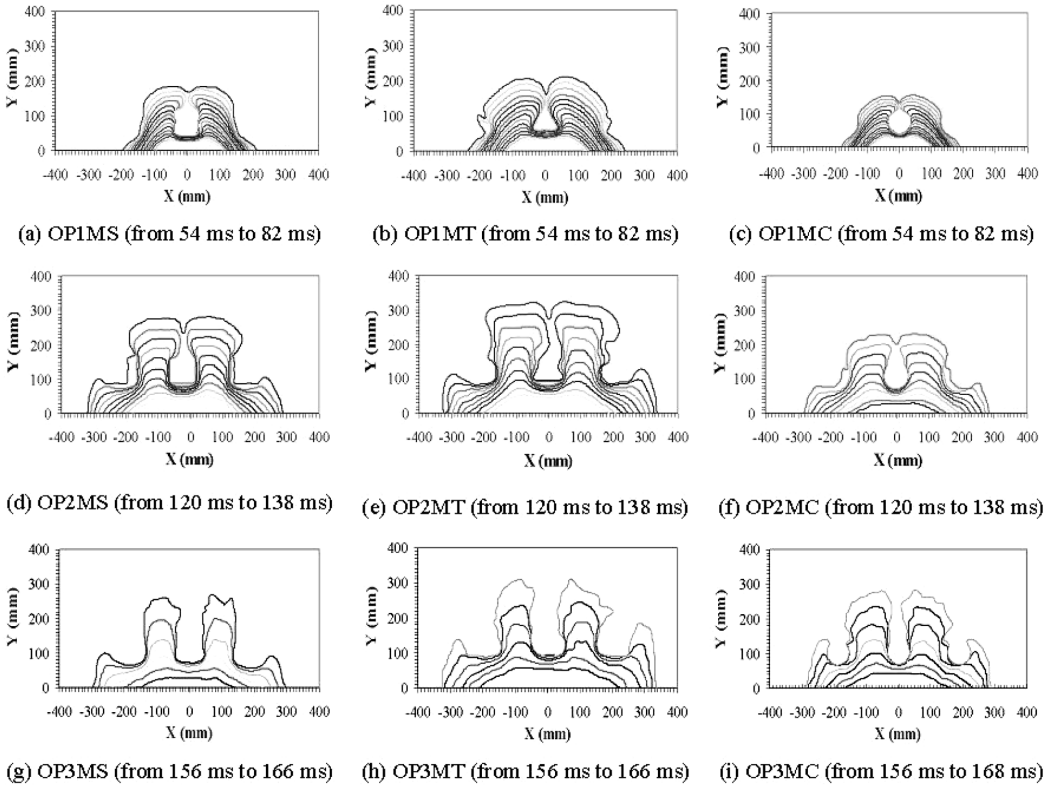

Fig. 3. A temporal sequence of flame-front images in the region of interest showing flame propagation around different multiple obstacles in different positions.

to 168 ms in Figs. 3(g)-(i).

From Figs. 2(a)-(c), during the early stage of flame propagation the flame propagates as a hemisphere around the chamber. As the flame front propagates towards the obstacles, the structure of the flame front begins to change. The local blockage caused by the presence of the obstacle causes the central region of the flame front to become flat. This phenomenon can be seen in Fig. 3. The leading flame front impinged on the closest face of the obstacle to the ignition point at about 54 ms (OP1), 120 ms (OP2) and 156 ms (OP3). The elapsed time for the passage of the flame front from the ignition point to the closest face of the obstacle was found to be similar for the three obstacle types. As the positions of obstacles were increased from 200, 500 mm to 800 mm in heights, the time taken from the ignition to the impingement on the central obstacle increased. The central surface becomes concave while the outer edges extend towards the openings on either side of the blockage. The flame front expands forcing the unburnt mixture to jet through the opening between the obstacles and between the outer obstacle and the wall of a chamber.

After impingement on the central obstacle, the two leading flame fronts develop through the space between the central obstacle and side obstacles. The flame continues to interact with multiple obstacles. With increasing time, the leading flame fronts reconnect in the wake of the central obstacle. Flame reconnection in the wake of central obstacle occurred at about 82 ms (OP1), 140 ms (OP2) and 160 ms (OP3). The flame reconnection times behind the different obstacles that were centrally placed within the chamber were found to be similar. It is clear that the time taken from the impingement on the central obstacle to the flame reconnection becomes faster in going from 200 mm, to 500 mm and to 800 mm in heights. During the flame reconnection, the flame continues to interact with the side obstacles with an increase in flame surface area. For the OP3 as the flame reconnects, it reached the chamber exit. Here, the flame contours outside the vent are not considered. For OP1, the travel time of the propagating flame front to the chamber exit occurred at about 144 ms (MT), 148 ms (MS) and 152 ms (MC) whereas it was at about 160 ms (MT), 164 ms (MS) and 168 ms (MC) for the OP3. The time taken to approach the chamber exit was found to be faster with obstacles at 200 mm height where the fastest time to the chamber exit was obtained with the triangular obstacles.

When compared with the time intervals taken from the flame impingement on the obstacle to the flame reconnection or to the chamber exit, the shorter time intervals occurred at 800 mm height while the longer was obtained from the height of 200 mm. This can be explained by the difference in the burnt gas contained between the bottom of chamber and the front face of obstacles to the ignition point which is shorter combustion time close to larger burnt gas.

3.2. Local Flame Displacement Speed

Local flame displacement speed, Sfd, was estimated

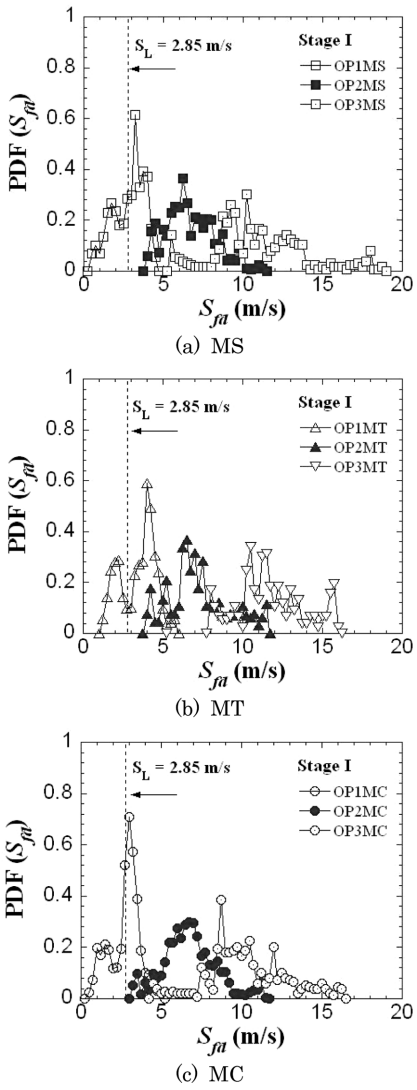

Fig. 4. PDFs of local flame displacement speed for stage I in different positions of multiple obstacles: (a) MS, (b) MT, (c) MC.

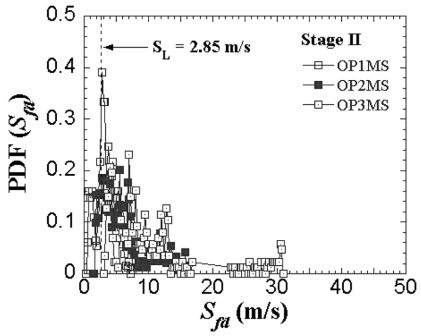

Fig. 5. PDFs of local flame displacement speed for stage II in different positions of multiple square obstacles.

along the flame front by dividing the distance along the normal line at each point by the time between two consecutive flame images. Here, any flame fronts touching the obstacle were excluded from the calculation of the displacement speed. Three different stages of flame propagation have been identified to govern the process of interaction between the flame and the obstacles.

The probability density functions (PDFs) of local flame displacement speed for the different obstacle geometries in different positions within the chamber are shown in Figs. 4-6. All the PDFs shown in the Figures were determined from all data points of flame contours presented in Fig. 3.

Stage I occurs as the flame approaches on the central obstacle. As the flame front approaches the obstacle, the central region ahead of the obstacle begins to deform. With the increasing time, the flame with a concaved nature develops towards the obstacle while the outside edges of the flame front extend towards the outside edges of the obstacle. As shown in Fig. 4, the PDFs during stage I of the OP1 exhibit a relatively narrow velocity distribution and are nearly symmetrical about 2.85 m/s, indicating laminar flame propagation. As the positions of obstacles are increased, the PDFs shift to higher values.

Stage II occurs as the flame interacts with the lateral sides of square obstacle, and the PDF's for this stage are shown in Fig. 5. The leading flame front interaction with vortices generated within the shear layer on the later sides of the square caused larger regions where $S_{fd} > 2.85$ m/s than in stage I. The OP1MS has a peak PDF of about 0.4 at 2.85 m/s.

This means there is little opportunity for the turbulence generation. The OP3MS has a noticeably

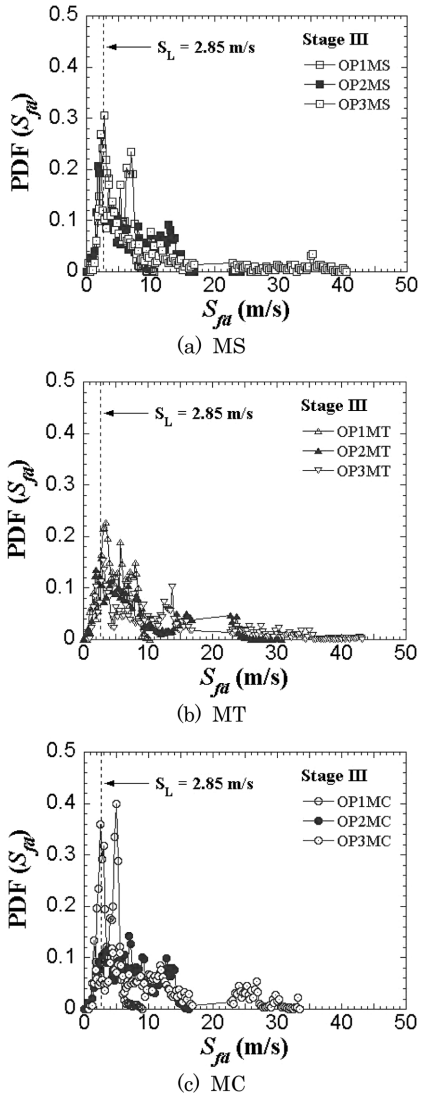

Fig. 6. PDFs of local flame speed for stage III in different positions of multiple obstacles: (a) MS, (b) MT, (c) MC.

longer tail with $S_{fd} > 20$ m/s. This tail is linked to flame acceleration generated caused by strong turbulence normal to the flame.

Stage III occurs as the flame front reconnects in the wake of the obstacle, and this stage is shown in Fig. 6. As the leading flame fronts propagate behind the central obstacle, the lateral propagating flame towards the side obstacles becomes concaved. This causes flame deceleration in that direction. Behind the obstacle, however, small-scale disturbances of the flow in the wake of the obstacle cause turbulence near the flame

front. Any flame-front turbulence normal to the direction of the propagating flame accelerates the flame normal to the direction of flow. A common feature to the local displacement speed PDFs in stage III is the shorter tail towards the lower speeds (S_{fd} < 2.85 m/s) and the longer tail towards S_{fd} > 20 m/s. Both of these attributes are the result of flame interaction with the central and side obstacles. The regions of lower speed are found where the flame becomes concave near the side obstacles. The distribution towards S_{fd} > 20 m/sis mainly caused by the acceleration of the leading flame behind the central obstacle. This phenomenon is similar to that seen in OP3MS stage II.

It can be also seen that the PDFs in OP3 are distributed mainly towards the higher values, and OP3 has also a lower peak PDF than those of OP1 and OP2. It is found that the triangular obstacles resulted in the higher local flame speeds while the lowest speeds were obtained with the circular obstacles.

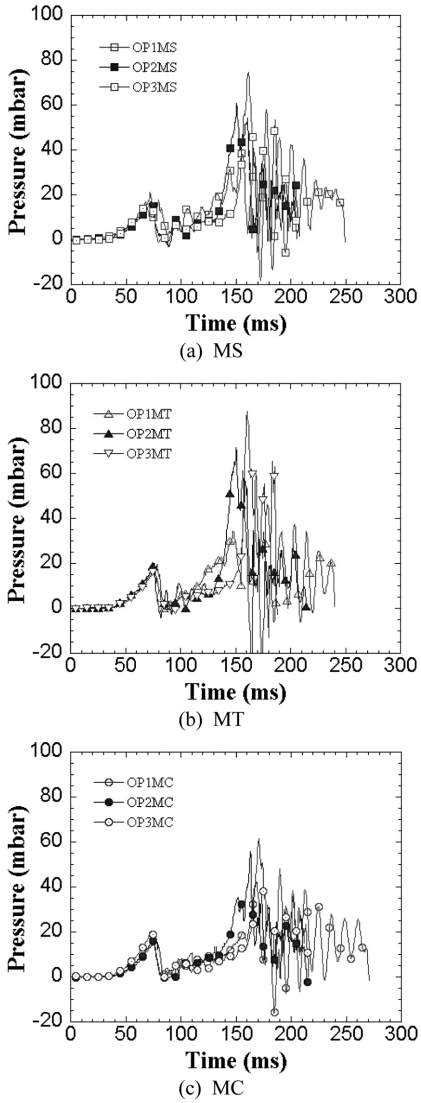

Fig. 7. Comparison of pressure-time history for the different positions within the same shapes of the obstacle geometries.

3.3. Pressure Development

Figs. 7(a)-(c) show the effect of height of the different multiple obstacles within the chamber. Two distinct pressure peaks occurred. The first peak is linked to the vent opening pressure, and the second one is linked to the overpressure generated in the chamber. As shown in the Figure, the first peak occurs at around 70 ms, regardless of the obstacle type and the height of the obstacles. The second peak pressure occurs as the flame front emerging from the vent ignites the unburned gas which has previously been expelled from the chamber, which results in a sharp increase in the internal pressure.

As the height of the obstacles was increased, the peak overpressure was also found to increase, regardless of the obstacle type. The peak pressure was dependent on the locations of obstacles. This is possibly due to increasing expansion effects of combustion through the bottom end as the positions of obstacles are increased further downstream. The highest overpressures were obtained with the triangular obstacles whereas the lowest was obtained with the cylindrical obstacles.

IV. Conclusions

The main findings obtained from the present study can be summarized as follows.

1. Faster flame propagation from the ignition to the vent occurred at 200 mm height while the slower was at 800 mm height. However, as compared with the time intervals taken from the flame impingement on the obstacles to the flame reconnection or to the chamber exit, the shorter time occurred at 800 mm height while the longer was obtained from the height of 200 mm. This is due to the difference in the burnt gas between the bottom of chamber and the obstacle. The fastest time to the chamber exit was obtained with the triangular bars, regardless of height of obstacles.

2. The local flame displacement is found to be proportional to height of multiple obstacles within the

chamber and is found to be higher for obstacles with triangular cross section. During stage IV, indicating the flame behaviour behind the obstacle, the local flame displacement speed PDFs were extensively distributed towards higher displacement speed than other stages. The triangular bar caused the higher pressure while the circular bar caused the lower pressures, regardless of the positions of obstacles. The peak pressure was found to be sensitive to the locations of obstacles.

References

[1] Moen, I.O., M. Donato, R. Knystautas and J.H.S. Lee, "Flame Acceleration Due to Turbulence Produced by Obstacles", *Combustion and Flame*, **39**, 21-32, (1980)

[2] Moen, I.O. and J.H.S. Lee, "Pressure Development Due to Turbulent Flame Propagation in Large-scale Methane-air Explosions", *Combustion and Flame*, **47**, 31-52, (1982)

[3] Hjertager, B.H., K. Fuhre and M. Bjorkhaug, "Concentration Effects on Flame Acceleration by Obstacles in Large-scale Methane-air and Propane-air Vented Explosions", *Combustion Science and Technology*, **62**, 239-256, (1988)

[4] Phylaktou, H. and G.E. Andrews, "Gas Explosions in Long Closed Vessels", *Combustion Science and Technology*, **77**, 27-39, (1991)

[5] Fairweather, M., G.K. Hargrave, S.S. Ibrahim and D.G. Walker, "Studies of Premixed Flame Propagation in Explosion Tubes", *Combustion and Flame*, **116**, 504-518, (1999)

[6] Hjertager, B.H., "Computer Modeling of Turbulent Gas Explosions in Complex 2D and 3D Geometries", *Journal of Hazardous Materials*, **34**, 173-197, (1993)

[7] Popat, N.R., C.A. Catlin, B.J. Arntzen, R.P. Lindstedt, B.H. Hjertager, T. Solberg, O. Saeter and A.C. Van den Berg, "Investigations to Improve and Assess the Accuracy of Computational Fluid Dynamics Based Explosion Models", *Journal of Hazardous Materials*, **45**, 1-25, (1996)

[8] Masri, A.R., S.S. Ibrahim, N. Nehzat and A.R. Green, "Experimental Study of Premixed Flame Propagation over Various Solid Obstructions", *Experimental Thermal and Fluid Science*, **21**, 109-116, (2000)

[9] Ibrahim, S.S. and A.R. Masri, "The Effects of Obstructions on Overpressure Resulting from Premixed Flame Deflagration", *Journal of Loss Prevention in the Process Industries*, **14**, 213-221, (2001)

[10] Ibrahim, S.S., G.K. Hargrave and T.C. Williams, "Experimental Investigation of Flame/Solid Interactions in Turbulent Premixed Combustion", *Experimental Thermal and Fluid Science*, **24**, 99-106, (2001)

[11] Hargrave, G.K., S.J. Jarvis and T.C. Williams, "A Study of Transient Flow Turbulence Generation During Flame/Wall Interactions in Explosions", *Measurement Science and Technology*, **13**, 1036-1042, (2002)

[12] Park, D.J., A.R. Green, Y.S. Lee and Y.C. Chen, "Experimental Studies on Interactions between a Freely Propagating Flame and Single Obstacles in a Rectangular Confinement", *Combustion and Flame*, **150**, 27-39, (2007)